REPORT DOCUMENTATION PAGE

Form Approved OMB NO. 0704-0188

1. REPORT DATE (DD-MM-YYYY)	2. REPORT TYPE	3. DATES COVERED (From - To)
22-05-2013	Final Report	12-Dec-2011 - 11-Sep-2012

4. TITLE AND SUBTITLE
Final Report: Novel Processing for Creating 3D Architectured Porous Shape Memory Alloy

5a. CONTRACT NUMBER
W911NF-12-1-0013

5b. GRANT NUMBER

5c. PROGRAM ELEMENT NUMBER
611102

6. AUTHORS
L Catherine Brinson

5d. PROJECT NUMBER

5e. TASK NUMBER

5f. WORK UNIT NUMBER

7. PERFORMING ORGANIZATION NAMES AND ADDRESSES
Northwestern University Evanston Campus
Office for Sponsored Research (OSR)
1801 Maple Ave., Suite 2410
Evanston, IL 60201 -

8. PERFORMING ORGANIZATION REPORT NUMBER

9. SPONSORING/MONITORING AGENCY NAME(S) AND ADDRESS(ES)
U.S. Army Research Office
P.O. Box 12211
Research Triangle Park, NC 27709-2211

10. SPONSOR/MONITOR'S ACRONYM(S)
ARO

11. SPONSOR/MONITOR'S REPORT NUMBER(S)
61337-MS-II.6

12. DISTRIBUTION AVAILIBILITY STATEMENT
Approved for Public Release; Distribution Unlimited

13. SUPPLEMENTARY NOTES
The views, opinions and/or findings contained in this report are those of the author(s) and should not contrued as an official Department of the Army position, policy or decision, unless so designated by other documentation.

14. ABSTRACT
We have developed two processing methods for creating fully 3D interconnected NiTi porous structures with arrayed micro-channels. Processing with HIPing results in a fully densified matrix, though bonding at powder boundaries is limited by oxidation. the strength of the powder bonding can be increased by processing with liquid phase sintering, though the resulting matrix is not fully densified. Tailored to the specific application, both of these methods are valuable for creation of these 3D interconnected structures.

15. SUBJECT TERMS
shape memory alloy, powder metallurgy, digital image correlation, phase transformation

16. SECURITY CLASSIFICATION OF:			17. LIMITATION OF ABSTRACT	15. NUMBER OF PAGES	19a. NAME OF RESPONSIBLE PERSON
a. REPORT	b. ABSTRACT	c. THIS PAGE			L. Catherine Brinson
UU	UU	UU	UU		19b. TELEPHONE NUMBER: 847-467-2347

Standard Form 298 (Rev 8/98)
Prescribed by ANSI Std. Z39.18

Report Title

Final Report: Novel Processing for Creating 3D Architectured Porous Shape Memory Alloy

ABSTRACT

We have developed two processing methods for creating fully 3D interconnected NiTi porous structures with arrayed micro-channels. Processing with HIPing results in a fully densified matrix, though bonding at powder boundaries is limited by oxidation. the strength of the powder bonding can be increased by processing with liquid phase sintering, though the resulting matrix is not fully densified. Tailored to the specific application, both of these methods are valuable for creation of these 3D interconnected structures.

The stress-strain response of these types of samples was examined through digital image correlation. the Fully strain field around a single and multiple pores was examined and compared to continuum modeling of the same geometry. While the transformation is captured qualitatively as it initiates below the pores and propagates 45° to the applied tensile load, continuum modeling is unable to capture the discrete with multiple pores, as the transformation bands cross and interact during deformation. Therefore while continuum modeling will clearly illustrate the trends of the deformation, as pore size and spacing approaches the granular length scale, these discrete effects cannot be captured by continuum modeling but must be examined experimentally.

Enter List of papers submitted or published that acknowledge ARO support from the start of the project to the date of this printing. List the papers, including journal references, in the following categories:

(a) Papers published in peer-reviewed journals (N/A for none)

Received	Paper

TOTAL:

Number of Papers published in peer-reviewed journals:

(b) Papers published in non-peer-reviewed journals (N/A for none)

Received	Paper

TOTAL:

Number of Papers published in non peer-reviewed journals:

(c) Presentations

1. C Tupper, A Emery, A Neurohr, D Rowenhorst, LC Brinson, D Dunand. “Interconnected Porosity in Shape Memory NiTi Foams.” 7th International Conference on Porous Metals and Metallic Foams (MetFoam), Busan, Korea, September 18-21, 2011.
2. LC Brinson, C Tupper, A Stebner. "Local Phase Transformations in Porous NiTi Structures - microscale characterization and modeling." 48th Annual Technical Meeting of SES, Northwestern University, October 10-14, 2011.
3. Stebner, A. Brinson, L.C. “Micromechanics of NiTi Martensite: Advancements and Challenges” Oct 2011, 48th Meeting of SES, Northwestern University, Evanston, IL.
4. C Tupper, A Emery, A Neurohr, D Rowenhorst, LC Brinson, D Dunand. "Interconnected Porosity in Shape Memory NiTi Foams." 7th International Conference on Porous Metals and Metallic Foams (MetFoam), Busan, Korea, September 18-21, 2011.
5. Stebner, A. Krueger, J. Neurohr, A. Mabe, J. Brinson, L.C. “Light-weight, Fast-Cycling, Shape-Memory Actuation Structures” Sep 2011, ASME Conference on Smart Materials, Adaptive Structures, and Intelligent Systems, Phoenix, AZ, SMASIS2011-4988.
6. C Bewerse, LC Brinson, D Dunand. "3D Interconnected Channels in NiTiNb Foams." TMS 2013 142nd Annual Meeting and Exhibition, San Antonio, TX, March 3-7, 2013.
7. Stebner, A. Brinson, L.C. “Deformation Mechanics of NiTi Martensite: New Findings and Open Challenges” Feb 2013, TMS, San Antonio, TX.
8. C Bewerse, LC Brinson, D Dunand. “3D Interconnected Channels in NiTiNb Foams.” TMS 2013 142nd Annual Meeting and Exhibition, San Antonio, TX, March 3-7, 2013.

Number of Presentations: 8.00

Non Peer-Reviewed Conference Proceeding publications (other than abstracts):

Received	Paper

TOTAL:

Number of Non Peer-Reviewed Conference Proceeding publications (other than abstracts):

Peer-Reviewed Conference Proceeding publications (other than abstracts):

Received	Paper

TOTAL:

Number of Peer-Reviewed Conference Proceeding publications (other than abstracts):

(d) Manuscripts

Received	Paper	
05/22/2013	1.00	D.W. Brown, A.P. Stebner, L.C. Brinson. Measurement of elastic constants of monoclinic nickel-titanium and validation offirst principles calculations, Applied Phylics letters (02 2013)
05/22/2013	2.00	A.P. Stebner, L.C. Brinson. Explicit finite element implementation of an improved threedimensional constitutive model for shape memory alloys, Computer Methods in Applied Mechanics and Engineering (04 2013)
05/22/2013	3.00	A.P. Stebner, Donald W Brown, L Cate Brinson. Young's Modulus Evolution and Texture Based Elastic - Inelastic Strain Partitioning During LargeUniaxial Deformations of Monoclinic Nickel-Titanium, Acta Materiala (01 2013)
05/22/2013	4.00	Aaron Stebner, Ph.D., , Sven C Vogel, PhD, Ronald D Noebe, Ph.D., Thomas Sisneros, B.Sc., , Bjorn Clausen, Ph.D., Donald W Brown, Ph.D., Anita Garg, Ph.D., L.Catherine Brinson, Ph.D.. Micromechanical Elastic, Twinning, and Slip Strain Partitioning ofPolycrystalline, Monoclinic Nickel-Titanium Large Uniaxial DeformationsMeasured via In Situ Neutron Diffraction, Journal of the Mechanics and Physics of Solids (12 2012)
05/22/2013	5.00	Catherine Bewerse , Keith R. Gall, Gavin J. McFarland , Pingping Zhu , L.Catherine Brinson. Local and global strains and strain ratios in shape memoryalloysusing digitalimagecorrelation, Materials Science and Engineering A ( )
TOTAL:	**5**	

Number of Manuscripts:

Books

Received	Paper
TOTAL:	

Patents Submitted

Patents Awarded

Awards

Graduate Students

NAME	PERCENT_SUPPORTED	Discipline
Aaron P Stebner	1.00	
Pingping Zhu	0.30	
FTE Equivalent:	**1.30**	
Total Number:	**2**	

Names of Post Doctorates

NAME	PERCENT_SUPPORTED
New Entry	0.00
FTE Equivalent:	**0.00**
Total Number:	**1**

Names of Faculty Supported

NAME	PERCENT_SUPPORTED
FTE Equivalent:	
Total Number:	

Names of Under Graduate students supported

NAME	PERCENT_SUPPORTED
FTE Equivalent:	
Total Number:	

Student Metrics

This section only applies to graduating undergraduates supported by this agreement in this reporting period

The number of undergraduates funded by this agreement who graduated during this period:	0.00
The number of undergraduates funded by this agreement who graduated during this period with a degree in science, mathematics, engineering, or technology fields:.....	0.00
The number of undergraduates funded by your agreement who graduated during this period and will continue to pursue a graduate or Ph.D. degree in science, mathematics, engineering, or technology fields:.....	0.00
Number of graduating undergraduates who achieved a 3.5 GPA to 4.0 (4.0 max scale):	0.00
Number of graduating undergraduates funded by a DoD funded Center of Excellence grant for Education, Research and Engineering:	0.00
The number of undergraduates funded by your agreement who graduated during this period and intend to work for the Department of Defense	0.00
The number of undergraduates funded by your agreement who graduated during this period and will receive scholarships or fellowships for further studies in science, mathematics, engineering or technology fields:	0.00

Names of Personnel receiving masters degrees

NAME
Total Number:

Names of personnel receiving PHDs

NAME
Total Number:

Names of other research staff

NAME	PERCENT SUPPORTED
Gavin McFarland	1.00
Catherine Tupper	1.00
FTE Equivalent:	**2.00**
Total Number:	**2**

Sub Contractors (DD882)

Inventions (DD882)

Scientific Progress

Problem Studied

Processing of NiTi alloys has been well developed for commercial production of monolithic bars, sheets, rods, wired, and tubing. However, available processing methods for porous NiTi structures have been limited to either fully control pore distribution and shape with 2D interconnected channels, [1,2] or to create fully interconnected porosity with randomly dispersed, equiaxed pores [3,4]. In this project we developed a novel processing technique for fabrication of regular arrays of three-dimensionally interconnected microchannels. This method is based on embedding steel wires in NiTi that are subsequently removed by electrochemical dissolution to create the ordered micro-channel arrays in a dense NiTi structure.

These arrayed porous structures are less computationally expensive than random porosity foams to model with finite element modeling. However, as the pore size and spacing approaches the granular length scale, it is unknown how well continuum modeling will represent the discrete granular response in confined NiTi domains. Therefore we also studied the kinetics of the phase transformation in confined domains. We characterized the strain field around single and multiple pores using a combination of digital image correlation (DIC) and mechanical testing. These results were compared to finite element modeling to reveal the local and global mechanical aspects of the SMA response.

Summary of Important Results

Fabrication of 3D interconnected NiTi structures

To create NiTi porous structures with organized arrays of micro-channels, steel wires were used as a spaceholder with powder metallography. High carbon steel wires were chosen with a wire diameter of 400 μm. The wires were orthogonally stacked with 500 μm spacing between wires in each layer, as shown in Figure 1a. (see attachment) After stacking, the spaceholder frame was sintered together at 960°C for 4 hr under vacuum to ensure connectivity between the wires. The frame was then packed with pre-alloyed NiTi powders with a nominal composition of 48.6 at% Ni sieved to a size range of 44-106 μm. The composite structure was densified with hot isostatic pressing for 3.5 hr at 40 MPa and 1020°C under vacuum.

The steel wires were then removed from the structure using electrochemical dissolution. NiTi is more noble than carbon steel, so is galvanically protected while the steel is selectively dissolved. The sample is attached to a Ti anode in a electrolyte bath of supersaturated NaCl with 3% acetic acid in deionized water. A 1.2 V voltage bias was then used to dissolve the steel while ultra-sonication is used to remove the dissolution product and refresh the electrolyte at the surface.

High carbon steel wires were chosen for protection of the NiTi matrix during dissolution. It has been shown [1,5] that unless the inter-diffusion of Fe into the NiTi matrix is prevented, a portion of the matrix will also be dissolved. However, in the presence of small amounts of carbon a TiC layer will readily form between the wire spaceholder and the NiTi matrix. This fully prevents inter-diffusion of Fe into the NiTi matrix. Previously, steel spaceholders were carburized before processing. In this case, high carbon steel wire was used to eliminate the need for this step. The TiC layer was readily formed, as shown in Figure 1b (see attachment), and the wires were well replicated into micro-channels after dissolution.

The resulting structure has well replicated channels with 60% open porosity and ~0.5% closed porosity as shown in Figure 2a. (see attachement) At the hot pressing temperatures, the steel wires were soft and distorted. The resulting channels have and aspect ratio of 0.76, with a 435 μm major axis and a 365 μm minor axis as illustrated in Figure 2b. (see attachment) The hot pressing direction is illustrated along the thick yellow arrow. The original wire cross sections are indicated with dashed red circles. The channels are fully connected in the third dimension through interconnection windows illustrated in Figure 2c. (see attachment) While theoretically the wires are only connected at a single point, the distortion of the wires, as well as the inability of the NiTi powders to fully pack into the wire junction, allows for larger interconnection windows. In fact, the windows are approximately 360 μm in diameter, or ¾ the size of the micro-channels directly created by the spaceholder. The porous structure can be viewed as columns in parallel connected by strut bridges.

The structure was characterized with increasing cyclic compression. The structure was compressed to a predetermined load, removed from the machine and heated above 100°C for 5 minutes, cooled down below 0°C for 5 minutes, then loaded to the next loading step. The heat treatment was to ensure that the samples are fully martensitic before each compression cycle. The structure has relatively low stiffness and strength, as shown in the stress-strain graph in Figure 3a. (see attachement) The structure has a stiffness of approximately 15 GPa, and fractured after 0.64% strain at 88 MPa. Examination of the fracture surface shows that fracture occurred in the loaded columns, as opposed to the connecting struts, with cracking along powder boundaries (Figure 3b). (see attachment) While the structure was fully densified, bonding between NiTi powders in the matrix is limited by oxides on the surface. This is why cracking initiates at the boundaries.

In order to increase the strength of bonding at the powder boundaries, a second processing technique was developed. Rather than bonding the NiTi powders together with HIPing, liquid phase sintering was

used. At 1150°C Nb forms a eutectic with binary NiTi. This eutectic is very reactive and dissolves oxides into the formed liquid. The oxides are redeposited as intermetallics at the powder boundaries, but have been shown not to adversely affect the mechanical properties [6]. The eutectic phase has been shown to have high tensile strength
bonding [7], and high wettability of NiTi. The liquid eutectic wicks into space between powder particles, liquid sintering them together upon solidification.

The liquid phase sintering processing method is similar to the method detailed above, in that a composite of NiTi powders and a steel spaceholder frame is created, and the frame is electrochemically removed. However, the alternate densification method changed several aspects of the processing, which is illustrated schematically in Figure 4. (see attachment) Tubes were used rather
than wires to reduce the dissolution time. The electrolyte can flood tubes during dissolution, allowing the spaceholder to dissolved radially rather than axially dissolved wires. Stainless steel tubes are available commercially, so were used as the spaceholder. Also, 5.3 wt% Nb powder is blended with the NiTi powder matrix to form small amounts of the eutectic phase.

The tubes were carburized and sensitized to enable dissolution. During this process, chromium carbides form at the grain boundaries, removing the stainless corrosion protection of chromium oxide at the grain boundaries. This rapidly decreased the dissolution time by an order of magnitude. However, the presence of eutectic reactions complicated the heat treatment processes. There is a eutectic reaction between Ni-Ti-Fe at 1100°C, which is below the Ni-Ti-Nb eutectic reaction at 1150°C. Therefore, the steel tube spaceholders must be removed before the matrix can be densified.

The frame is again formed with orthogonal stacking of the stainless steel tubes, which are 400 μm in diameter and spaced by 500 μm. The frame was sintered together at 1050°C for 48 hr under argon, followed by carburizing for 960°C for 4 hr packed in graphite under flowing argon. The NiTi+Nb powder blend was then packed around the frame and cold compacted to 300 MPa. The structure was sintered under high vacuum at 1020°C for 24 hr to stabilize it for dissolution of the frame, and then the frame was sensitized at 600°C for 1 hr while cooling. The stainless steel tubes were electrochemically dissolved as described above, though the electrolyte was supersaturated NaCl in deionized water under a 1.5 V potential bias. Finally, the structure was sintered at 1140°C for 30 minutes, followed by liquid phase sintered at 1180°C for 30 minutes under high vacuum.

The micro-channels are well formed after dissolution of the stainless steel tubes and liquid phase sintering of the NiTi matrix. Figure 5a (see attachment) illustrates the micro-channels with insets showing the continuity of the channels through the structure and the interconnected NiTi matrix. The yellow arrow indicates the cold compaction direction. In the matrix, NiTi powders are connected by NiTi-Nb eutectic bridges. When the eutectic is formed, the liquid wicks into the structure, leaving behind a roughened surface texture where the NiTi powders are clearly visible on the surface. As the liquid wicks away from the channels and into the matrix, it also slightly enlarges the cross section of the micro-channels. This is opposite the case of HIPing, where the NiTi powders are pressed into the softer steel wire slightly decreasing the cross section of the micro-channels (distortion aside).

A cross section of the liquid phase sintered structure in Figure 5b (see attachment) shows that the channels are uniform in diameter though the length of the sample. The matrix is not fully densified, but contains ~16% porosity, which is a combination of open and closed. A second cross section rotated 90° in Figure 5c (see attachment) illustrates the regular array of channels. The rough texture from the liquid phase sintering causes the irregular cross section of the channels, though on average they are circular. Finally in Figure 5d the interconnection windows are clearly visible. Again the windows are approximately ¾ the size of the channels with a diameter of ~360 μm. This second processing method also creates porosity of arrayed micro-channels fully interconnected in three dimensions.

Technology Transfer

Final Report: Novel Processing for Creating 3D Architectured Porous Shape Memory Alloy

L. Catherine Brinson
Northwestern University
March 2013

Problem Studied

Processing of NiTi alloys has been well developed for commercial production of monolithic bars, sheets, rods, wired, and tubing. However, available processing methods for porous NiTi structures have been limited to either fully control pore distribution and shape with 2D interconnected channels, [1,2] or to create fully interconnected porosity with randomly dispersed, equiaxed pores [3,4]. In this project we developed a novel processing technique for fabrication of regular arrays of three-dimensionally interconnected microchannels. This method is based on embedding steel wires in NiTi that are subsequently removed by electrochemical dissolution to create the ordered micro-channel arrays in a dense NiTi structure.

These arrayed porous structures are less computationally expensive than random porosity foams to model with finite element modeling. However, as the pore size and spacing approaches the granular length scale, it is unknown how well continuum modeling will represent the discrete granular response in confined NiTi domains. Therefore we also studied the kinetics of the phase transformation in confined domains. We characterized the strain field around single and multiple pores using a combination of digital image correlation (DIC) and mechanical testing. These results were compared to finite element modeling to reveal the local and global mechanical aspects of the SMA response. Improvements to the constitutive modeling in finite elements were made based on neutron diffraction studies, which clarified the Young's modulus evolution of martensite during phase transformation and contributions of elastic, twinning and plastic strain to response.

Summary of Important Results

Fabrication of 3D interconnected NiTi structures

To create NiTi porous structures with organized arrays of micro-channels, steel wires were used as a spaceholder with powder metallography. High carbon steel wires were chosen with a wire diameter of 400 μm. The wires were orthogonally stacked with 500 μm spacing between wires in each layer, as shown in Figure 1a. After stacking, the spaceholder frame was sintered together at 960°C for 4 hr under vacuum to ensure connectivity between the wires. The frame was then packed with pre-alloyed NiTi powders with a nominal composition of 48.6 at% Ni sieved to a size range of 44-106 μm. The composite structure was densified with hot isostatic pressing for 3.5 hr at 40 MPa and 1020°C under vacuum.

The steel wires were then removed from the structure using electrochemical dissolution. NiTi is more noble than carbon steel, so is galvanically protected while the steel is selectively dissolved. The sample is attached to a Ti anode in a electrolyte bath of supersaturated NaCl with 3% acetic acid in deionized water. A 1.2 V voltage bias was then used to dissolve the steel while ultra-sonication is used to remove the dissolution product and refresh the electrolyte at the surface.

High carbon steel wires were chosen for protection of the NiTi matrix during dissolution. It has been shown [1,5] that unless the inter-diffusion of Fe into the NiTi matrix is prevented, a portion of the matrix will also be dissolved. However, in the presence of small amounts of carbon a TiC layer will readily form between the wire spaceholder and the NiTi matrix. This fully prevents inter-diffusion of Fe into the NiTi matrix. Previously, steel spaceholders were carburized before processing. In this case, high carbon steel wire was used to eliminate the need for this step. The TiC layer was readily formed, as shown in Figure 1b, and the wires were well replicated into micro-channels after dissolution.

a) 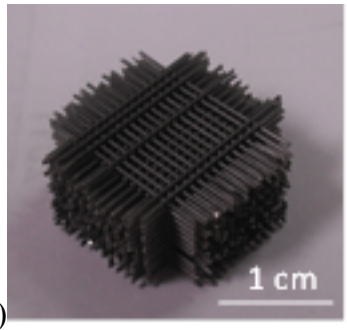

b) 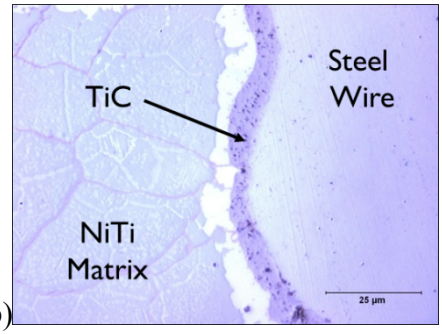

Figure 1. a) orthogonally stacked high carbon steel wire spaceholder frame and b) TiC layer between the spaceholder and matrix preventing inter-diffusion of Fe into the NiTi matrix.

The resulting structure has well replicated channels with 60% open porosity and ~0.5% closed porosity as shown in Figure 2a. At the hot pressing temperatures, the steel wires were soft and distorted. The resulting channels have and aspect ratio of 0.76, with a 435 µm major axis and a 365 µm minor axis as illustrated in Figure 2b. The hot pressing direction is illustrated along the thick yellow arrow. The original wire cross sections are indicated with dashed red circles. The channels are fully connected in the third dimension through interconnection windows illustrated in Figure 2c. While theoretically the wires are only connected at a single point, the distortion of the wires, as well as the inability of the NiTi powders to fully pack into the wire junction, allows for larger interconnection windows. In fact, the windows are approximately 360 µm in diameter, or ¾ the size of the micro-channels directly created by the spaceholder. The porous structure can be viewed as columns in parallel connected by strut bridges.

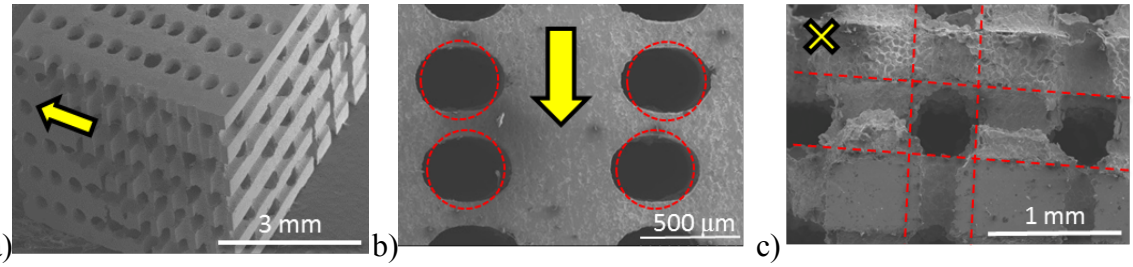

Figure 2. a) NiTi porous structure with 3D interconnected micro-channels, b) wired are distorted during HIPing, creating oblong microchannels, and c) the channels are fully interconnected in three dimensions. The HIPing direction is indicated by the yellow arrows, or the yellow X into the page. The red dashed lines in c) illustrate the micro-channels replicated from dissolved wires.

The structure was characterized with increasing cyclic compression. The structure was compressed to a predetermined load, removed from the machine and heated above 100°C for 5 minutes, cooled down below 0°C for 5 minutes, then loaded to the next loading step. The heat treatment was to ensure that the samples are fully martensitic before each compression cycle. The structure has relatively low stiffness and strength, as shown in the stress-strain graph in Figure 3a. The structure has a stiffness of approximately 15 GPa, and fractured after 0.64% strain at 88 MPa. Examination of the fracture surface shows that fracture occurred in the loaded columns, as opposed to the connecting struts, with cracking along powder boundaries (Figure 3b). While the structure was fully densified, bonding between NiTi powders in the matrix is limited by oxides on the surface. This is why cracking initiates at the boundaries.

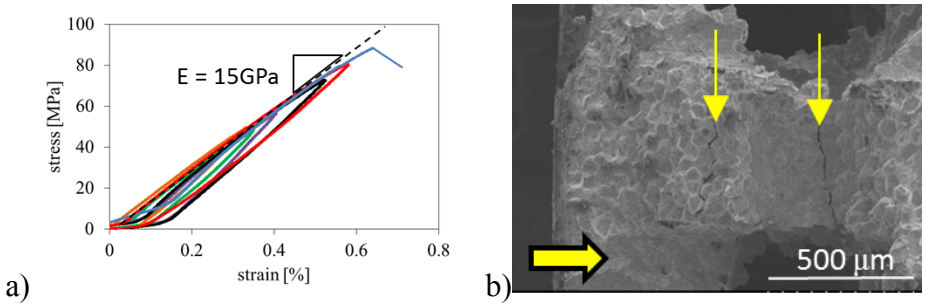

Figure 3. a) stress-strain of the NiTi structure under cyclic compression, b) fracture surface of the structure with cracking along powder boundaries illustrated with thin yellow arrows

In order to increase the strength of bonding at the powder boundaries, a second processing technique was developed. Rather than bonding the NiTi powders together with HIPing, liquid phase sintering was used. At 1150°C Nb forms a eutectic with binary NiTi. This eutectic is very reactive and dissolves oxides into the formed liquid. The oxides are redeposited as intermetallics at the powder boundaries, but have been shown not to adversely affect the mechanical properties [6]. The eutectic phase has been shown to have high tensile strength bonding [7], and high wettability of NiTi. The liquid eutectic wicks into space between powder particles, liquid sintering them together upon solidification.

The liquid phase sintering processing method is similar to the method detailed above, in that a composite of NiTi powders and a steel spaceholder frame is created, and the frame is electrochemically removed. However, the alternate densification method changed several aspects of the processing, which is illustrated schematically in Figure 4. Tubes were used rather than wires to reduce the dissolution time. The electrolyte can flood tubes during dissolution, allowing the spaceholder to dissolved radially rather than axially dissolved wires. Stainless steel tubes are available commercially, so were used as the spaceholder. Also, 5.3 wt% Nb powder is blended with the NiTi powder matrix to form small amounts of the eutectic phase.

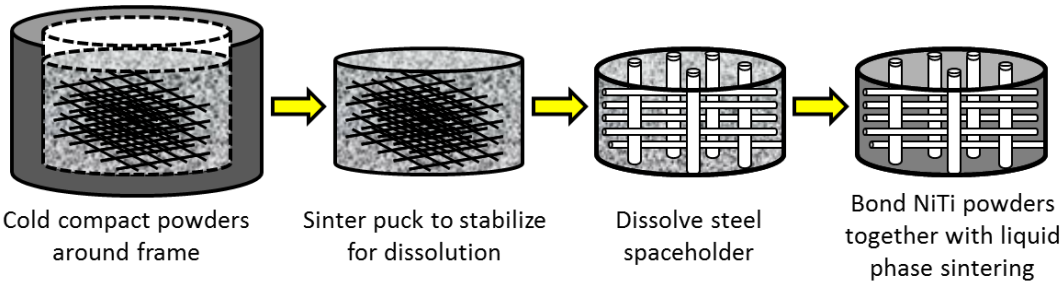

Figure 4. Processing steps for liquid phase sintering densification of NiTi structure with 3D interconnected porosity

The tubes were carburized and sensitized to enable dissolution. During this process, chromium carbides form at the grain boundaries, removing the stainless corrosion protection of chromium oxide at the grain boundaries. This rapidly decreased the dissolution time by an order of magnitude. However, the presence of eutectic reactions complicated the heat treatment processes. There is a eutectic reaction between Ni-Ti-Fe at 1100°C, which is below the Ni-Ti-Nb eutectic reaction at 1150°C. Therefore, the steel tube spaceholders must be removed before the matrix can be densified.

The frame is again formed with orthogonal stacking of the stainless steel tubes, which are 400 μm in diameter and spaced by 500 μm. The frame was sintered together at 1050°C for 48 hr under argon, followed by carburizing for 960°C for 4 hr packed in graphite under flowing argon. The NiTi+Nb powder blend was then packed around the frame and cold compacted to 300 MPa. The structure was sintered under high vacuum at 1020°C for 24 hr to stabilize it for dissolution of the frame, and then the frame was sensitized at 600°C for 1 hr while cooling. The stainless steel tubes were electrochemically dissolved as described above, though the electrolyte was supersaturated NaCl in deionized water under a 1.5 V potential bias. Finally, the structure was sintered at 1140°C for 30 minutes, followed by liquid phase sintered at 1180°C for 30 minutes under high vacuum.

The micro-channels are well formed after dissolution of the stainless steel tubes and liquid phase sintering of the NiTi matrix. Figure 5a illustrates the micro-channels with insets showing the continuity of the channels through the structure and the interconnected NiTi matrix. The yellow arrow indicates the cold compaction direction. In the matrix, NiTi powders are

connected by NiTi-Nb eutectic bridges. When the eutectic is formed, the liquid wicks into the structure, leaving behind a roughened surface texture where the NiTi powders are clearly visible on the surface. As the liquid wicks away from the channels and into the matrix, it also slightly enlarges the cross section of the micro-channels. This is opposite the case of HIPing, where the NiTi powders are pressed into the softer steel wire slightly decreasing the cross section of the micro-channels (distortion aside).

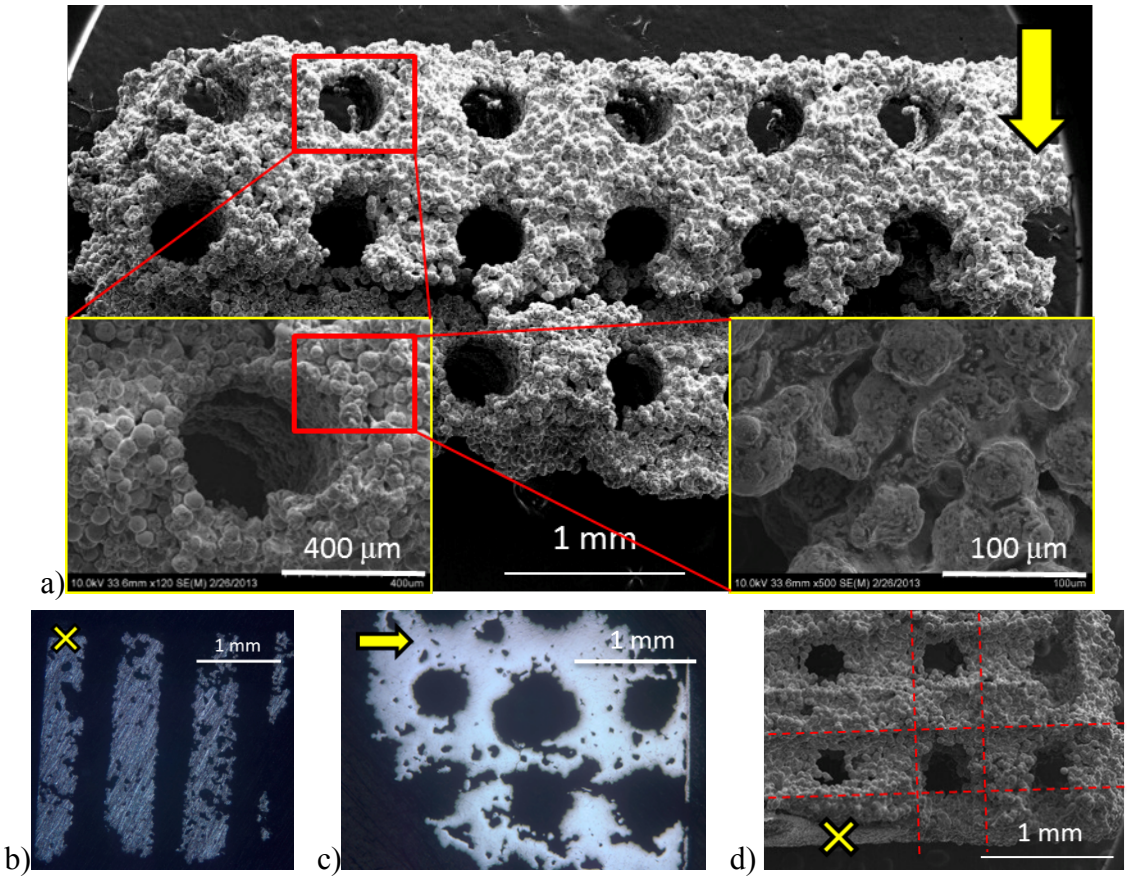

Figure 5. a) NiTi 3D porous structure densified with liquid phase sintering, b) cross section along one of the micro-channel directions where the yellow X indicates the cold compaction direction into the page, c) cross section perpendicular to one of the micro-channel directions, and d) interconnection windows forming the fully 3D porosity interconnection

A cross section of the liquid phase sintered structure in Figure 5b shows that the channels are uniform in diameter though the length of the sample. The matrix is not fully densified, but contains ~16% porosity, which is a combination of open and closed. A second cross section rotated 90° in Figure 5c illustrates the regular array of channels. The rough texture from the liquid phase sintering causes the irregular cross section of the channels, though on average they are circular. Finally in Figure 5d the interconnection windows are clearly visible. Again the windows are approximately ¾ the size of the channels with a diameter of ~360 µm. This second

processing method also creates porosity of arrayed micro-channels fully interconnected in three dimensions.

Analysis of the strain field around single and multiple pores

To further understand the macroscopic stress-strain response of these microchannel samples, the strain field around a single [8] and multiple pores was examined using digital image correlation (DIC). DIC outputs two dimensional maps of the axial and transverse strain field. These can be directly compared to strain field maps produced through finite element modeling. The shape memory response can be assessed using the Stebner-Brinson SMA continuum model based on the micromechanical reorientation of martensitic variants [9]. Experimentally, there are discrete granular effects that cannot be captured with the continuum model.

Around a single pore, the strain initiates directly below the hole with tensile deformation along the labeled x axis. The sample is a superelastic NiTi dogbone sample viewed under 5x magnification under an optical microscope. A single 0.5mm pore has been machined into the center of the gage section, around which the strain field was examined. The sample is strained to 1% axial strain in these figures. Strain radiates in lobes approximately 45° from the loading axis, which is well captured in the model and experimentally in Figures 6a and 6b. An optical micrograph of the polished surface during deformation in Figure 6c shows the transformed martensite in the disturbed microstructure. When the DIC strain field map is overlaid on the polished surface in 6b the high strain regions align well with the disturbed microstructure.

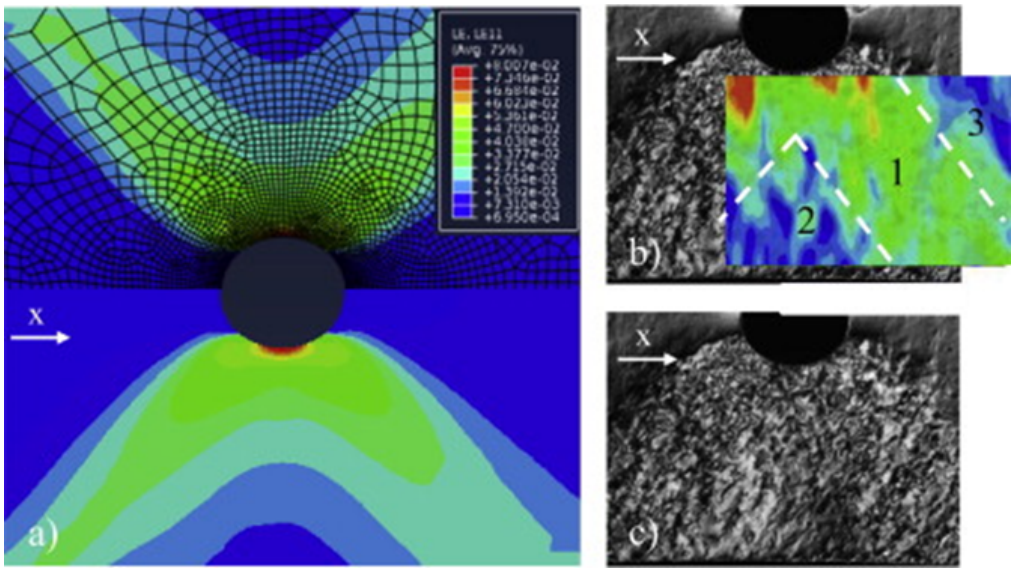

Figure 6. a) axial strain field map calculated using the Stebner-Brinson model in ABAQUS, b)optical image of the polished surface under 1% average global strain with and c) without overlaid DIC axial strain field map corresponding to the same global strain.

As DIC creates both axial and transverse strain field maps, a localized strain ratio can be calculated around the pore in Figure 7c. These localized strain ratio maps can also be calculated using the Stebner-Brinson SMA model (figure 7b), as well as linearly-elastic deformation in finite element modeling (Figure 7a). The localized strain ratio is not a Poisson's Ratio due to the non-uniaxial load state near the pore, but is the transverse strain field map divided by the axial strain field map. The discrete granular nature is unable to be captured with continuum modeling. However, qualitatively the lower localized strain ratio in region 3 is captured. This highly discrete nature of the deformation makes regions 1 and 2 difficult to compare directly to continuum modeling.

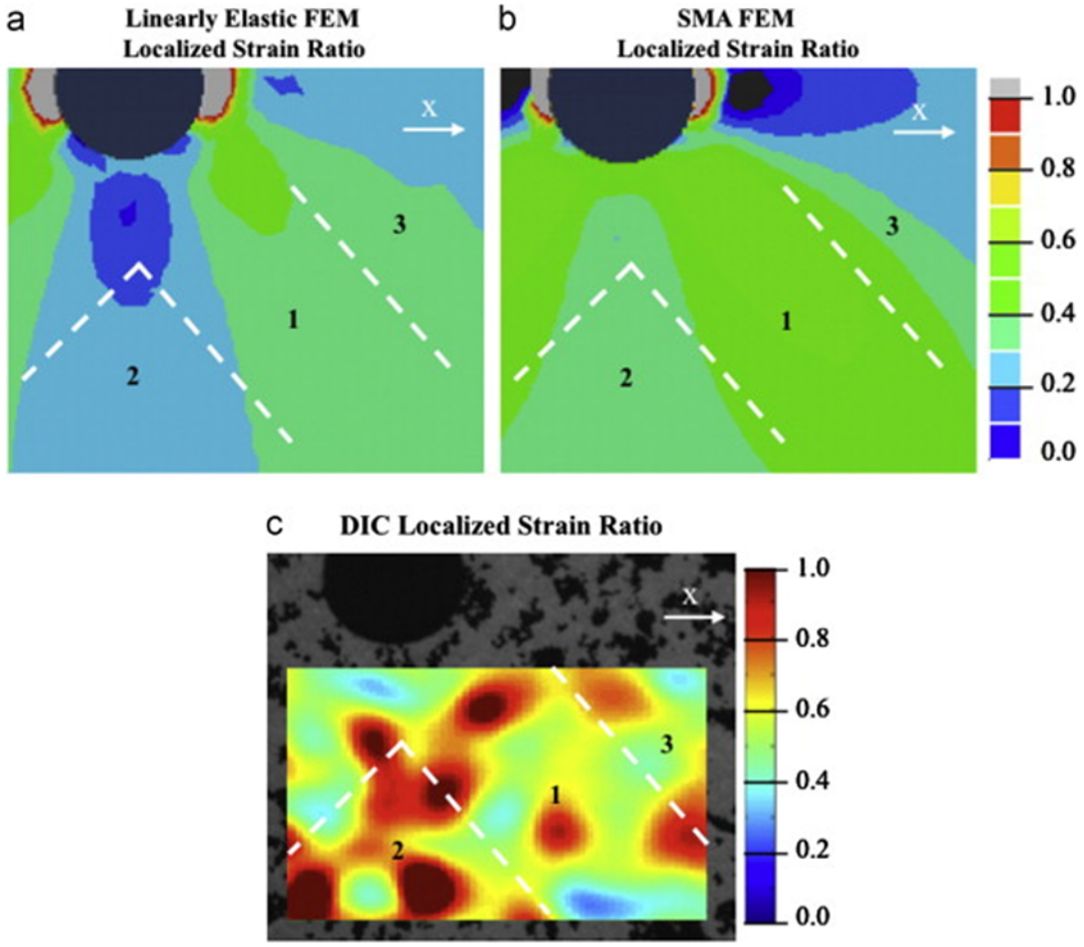

Figure 7. Full field localized strain ratio maps calculated with a) linear elastic FEM, b) Stebner-Brinson SMA FEM, and c) DIC

The same method can be used to study the interaction of two pores. In this dogbone sample of superelastic NiTi, two 0.5 mm pores were machined into the center of the gage section with 0.5 mm spacing between the pores. Strain still initiates below the pores, and propagates in 45° lobes with respect to the loading axis. However, the localized strain intensity is much higher with two pores in close proximity, as the strain fields from each pore begin interacting with each

other. With discrete granular deformation, the strain fields become very convoluted. The axial (Figure 8a) and transverse (Figure 8b) strain field maps are complementary, but not exactly inverse, as certain grains are aligned well for one direction or the other. In Figure 8c the right half of the axial strain field map is overlaid on the polished surface, both at 1% global strain. The discrete strain in the strain field map aligns well with the disturbed microstructure on the polished surface. The high strain in the DIC axial strain field map matches the highly transformed (disturbed) regions, while the low strain matches the untransformed regions.

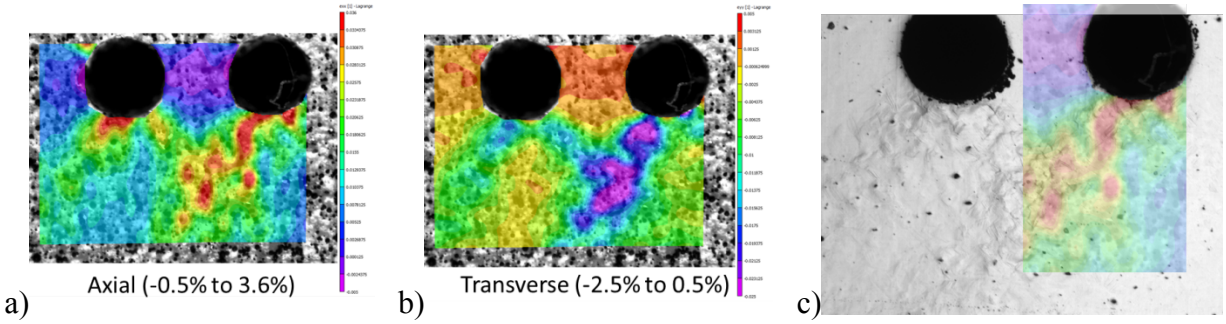

a) b) c)

Figure 8. a) axial and b) transverse strain field maps at 1% global strain, and c) the axial strain field map overlaid on the disturbed microstructure of the polished surface

Modeling and Micromechanical Response

A robust finite element implementation of a constitutive model for shape memory alloys was created [9]. This model was then used to study material vs. structural mechanics of pores and pore interactions in SMAs [12]. We also performed neutron diffraction experiments to study the micromechanical response of monoclinic NiTi. We developed new analysis methodologies for extracting volume fractions of the polycrystalline material that participate in individual twinning events from the diffraction data (Fig 9a-c, [11,13]). Through this work, we have been able to empirical study elastic, transformation, and plastic strain partitioning of this material (see Fig 9d, [10], [11]). We have also documented Young's modulus evolution of monoclinic NiTi subjected to large tensile and compressive deformation [10], empirically measured anisotropic elastic constants of monoclinic NiTi and used our measurements to validate first principles predictions [13], and quantified the contribution of active deformation twinning modes within monoclinic NiTi subjected to tension and compression [11].

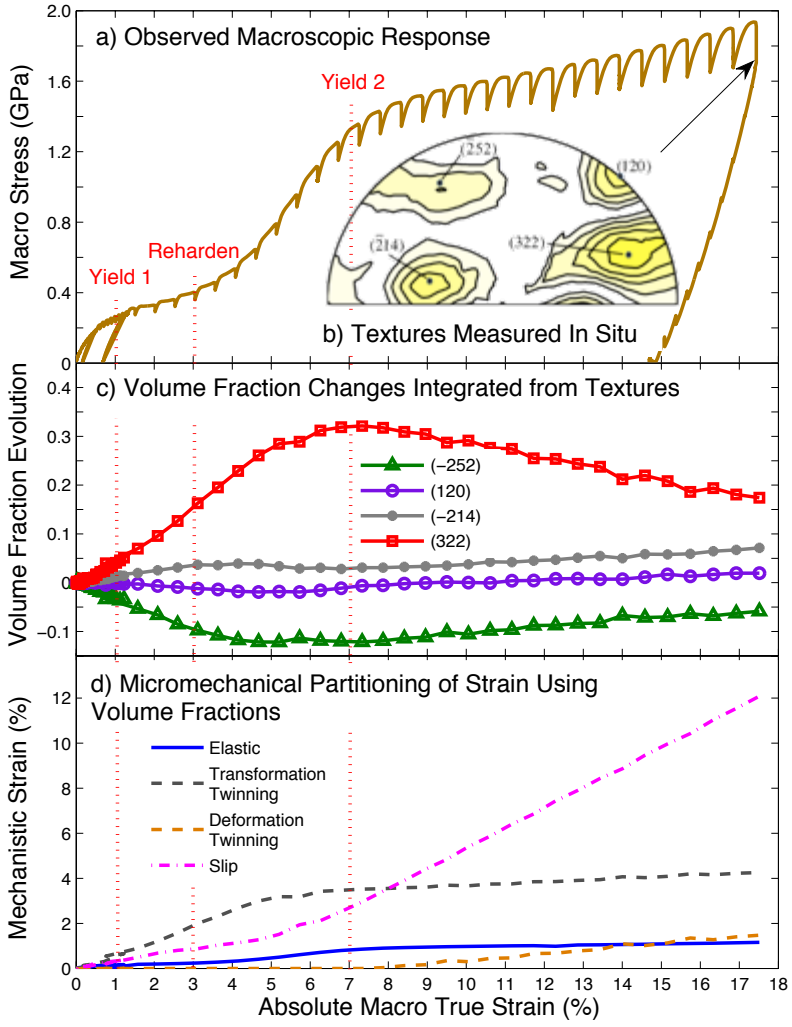

Figure 9. Elastic-inelastic strain partitioning of the macroscopic flow behavior of NiTi from neutron diffraction experiments.

Conclusions

We have developed two processing methods for creating fully 3D interconnected NiTi porous structures with arrayed micro-channels. Processing with HIPing results in a fully densified matrix, though bonding at powder boundaries is limited by oxidation. The strength of the powder bonding can be increased by processing with liquid phase sintering, though the resulting matrix is not fully densified. Tailored to the specific application, both of these methods are valuable for creation of these 3D interconnected structures.

The stress-strain response of these types of samples was examined through digital image correlation. The full strain field around a single and multiple pores was examined and compared to continuum modeling of the same geometry. While the transformation is captured qualitatively as it initiates below the pores and propagates 45° to the applied tensile load, continuum modeling is unable to capture the discrete granular effects of the polycrystalline NiTi. The strain field becomes more complicated with multiple pores, as the transformation bands cross and interact

during deformation. Therefore while continuum modeling will clearly illustrate the trends of the deformation, as pore size and spacing approaches the granular length scale, these discrete effects cannot be captured by continuum modeling but must be examined experimentally or by micromechanical modeling. Improvements to modeling were developed, with work on both continuum models and analysis of diffraction experiments which lead to insight of micromechanical behavior.

List of Figures

Bibliography

[1] A.J. Neurohr, D.C. Dunand, Acta Biomaterialia 7 (2011) 1862–72.
[2] A.J. Neurohr, D.C. Dunand, Acta Materialia 59 (2011) 4616–4630.

[3] A Bansiddhi, D.C. Dunand, Acta Biomaterialia 4 (2008) 1996–2007.
[4] A Bansiddhi, D. Dunand, Intermetallics 15 (2007) 1612–1622.
[5] D.J. Jorgensen, D.C. Dunand, Acta Materialia 59 (2011) 640–650.
[6] A. Bansiddhi, D.C. Dunand, Journal of Materials Research 24 (2009) 2107–2117.
[7] D.S. Grummon, K.-B. Low, J. Foltz, J.A. Shaw, in:, American Institute of Aeronautics and Astronautics, 2007, pp. 1–7.
[8] C. Bewerse, K.R. Gall, G.J. McFarland, P. Zhu, L.C. Brinson, Materials Science and Engineering: A 568 (2013) 134–142.
[9] A. P. Stebner, L.C. Brinson, Computer Methods in Applied Mechanics and Engineering (2013).
[10] Stebner, A.P. Brown, D.W. Brinson, L.C. "Young's Modulus Evolution and Texture Based Elastic-Inelastic Strain Partitioning of Large Uniaxial Deformations of Monoclinic Nickel-Titanium" 2013, *Acta Materialia* 61:1944-1956.
[11] Stebner, A.P. Sisneros, T.A. Vogel, S. Clausen B. Brown, D.W. Garg, A. Noebe R.D. Brinson, L.C. "Micromechanical Elastic, Twinning, and Slip Strain Partitioning of Polycrystalline, Monoclinic Nickel-Titanium Large Uniaxial Deformations Measured via In Situ Neutron Diffraction" Submitted to *Journal of the Mechanics and Physics of Solids,* 2013.
[12] Zhu, P. Stebner, A.P. Brinson, L.C. "A Numerical Study of Defect Effects on Transformation Fields during Superelastic Deformation" To be submitted to *Smart Materials and Structures.*
[13] Stebner, A.P., Brown, D.W., Brinson L.C. "Measurement of elastic constants of monoclinic nickel-titanium and validation of first principles calculations" in press, Applied Physics Letters, 2013.